GRADIENT BOOSTING ENSEMBLED METHOD FOR IN-VIVO BRAIN TUMOUR CLASSIFICATION USING HYPERSPECTRAL IMAGES

Ganji Tejasree

Research scholar, Vellore Institute of Technology
Vellore-632014, Tamil Nadu, India.
ganji.tejasree2020@vitstudent.ac.in

Agilandeeswari L

Associate professor, Vellore Institute of Technology
Vellore-632014, Tamil Nadu, India.
agila.l@vit.ac.in

Abstract

In the past few years, the use of hyperspectral imaging for medicinal purposes has increased. Hyperspectral imaging is a trending topic in the remote sensing field. It is used to collect the spectral information present in the scene. Additionally, the combination of spectral and spatial data offers valuable data for classifying brain tumours. When combined with Machine Learning (ML) algorithms, HSI (Hyperspectral Imaging) can be utilised as a non-intrusive medical diagnosis tool. By using hyperspectral images in the medical field, we can classify cancers, tissues, blood vessels etc. This paper offers a gradient boosting based ensembled classification (MCGC) scheme for In-Vivo brain cancer classification. And also, a multi-scale CNN method feature extraction and graph-based clustering method for feature selection are applied to get accurate classification results. The dataset used for brain cancer classification is the In-Vivo brain cancer dataset. These dataset images are captured when the real-time brain tumour surgery was going on. Finally, we performed the experiment results of gradient boosting ensembled classification methods. Support vector machine (SVM) and Random Forest (RF) classification methods were used to compare the outcomes of classification. And in comparison, with the other existing methods, we got good outcomes.

***Keywords*: Hyperspectral Imaging; remote sensing; machine learning; In-Vivo brain cancer; feature selection; support vector machine; Random Forest Classifier.**

1. Introduction

Hyperspectral imaging is one, where high-resolution imaging collects both spatial and spectral data from an extensive variety of wavelengths across the electromagnetic spectrum. The most popular subject in the field of remote sensing right now is hyperspectral imaging. Hyperspectral imaging (HSI) is a method for capturing images of an object at many wavelengths and getting spectral data for each pixel [Wei, *et al*. (2019)]. It has many applications in agriculture, environment, food detection, and medical field etc., in the medical field like digital pathology, surgery visualization, tissue condition diagnosis, brain cancer detection, and skin cancer detection [Souza, *et al*. (2021)]. In medical imaging, in recent years hyperspectral images are giving the best results. due to the spectral and spatial properties of these images, the tumour in its early stages can be identified using hyperspectral imaging. When the patient is feeling unhealthy, in cancer stage 1 we can identify the cancer tumour by doing an MRI scanning of the patient's head [Sancho, *et al*. (2020)]. Development of the impressive, non-invasive, affordable medical diagnostic techniques is a leading challenge for researchers worldwide. In-vitro, ex-vivo, and in-vivo investigations i.e., whether the scene is obtained from a resected sample (in-vitro, ex-vivo) or directly collected from the patient have all exploited the ability to identify the components inside a gathered image (in vivo). In particular, there is an increasing interest in doing In-Vivo HSI processing during operations to aid in the differentiation of malignant and healthy tissues [Lazcano *et al*. (2019)].

A safe, noncontact, and label-free imaging technique must be created immediately to facilitate real-time tumour removal during neurosurgery. Hyperspectral imaging is a rapid, non-contact, non-ionizing, non-invasive, high-safety, and label-free imaging method. With the advancement of modern medical detection technology, surgeons may execute this challenging task without the use of contrast agents by using hyperspectral imaging [Khan, *et al*. (2018)]. HSIs can provide detailed spectrum information that reflects the unique physical

characteristics of the objects, as opposed to panchromatic and multispectral pictures, which can significantly increase the capacity to identify and categorise the targets. These days, guidance aids for brain tumour excision surgery are mostly provided by imaging techniques like computed tomography (CT), magnetic resonance imaging (MRI), and ultrasound [Hao, *et al.* (2020)]. These imaging techniques can't find in real-time and require a long time to discover. The creation of a secure, non-contact, and label-free imaging technique is currently urgently required to give trustworthy assistance for real-time tumour removal during neurosurgery [Andria, *et al.* (2009)].

Thanks to the technology enabling this continual growth, the application of hyperspectral imaging in the medical field has gradually expanded to become a research hotspot. Recently, hyperspectral imaging has begun to demonstrate encouraging results in the detection of cancer. For instance, a strategy based on minimum spanning forest (MSF) and support vector machine (SVM) classifiers can be used to distinguish cancer from healthy tissue using hyperspectral imaging [Pike, *et al.* (2015)] and a diverse inserting framework is presented [Ravi, *et al.* (2017)]. The following are the top four issues with in vivo hyperspectral imaging of the human brain (HSIs): 1) Large amounts of information and detailed characteristics, 2) an uneven label distribution, 3) a wide range in illumination, and 4) mixed materials in the backdrop. For instance, medical equipment and background are labelled as one class are just a few of the issues that need to be addressed. Most of the hyperspectral tumour detection models used today are built using traditional machine learning (ML) techniques [Wei, *et al*. (2015)]. These tumour identification techniques depend on the manual extraction of characteristics, which is labour-intensive, time-consuming, and vulnerable to subjectivity. Finding effective automatic feature extraction and categorization techniques is crucial for research [Wang, *et al.* (2020)].

To overcome this research in HSI categorization based on deep learning is being conducted in light of the development of deep learning technology, which, among other things, is fuelled by huge data and powerful computers [LeCun, *et al.* (2015)]. The deep learning model can automatically extract deep, abstract, and semantic information from a range of inputs. Combining straightforward yet nonlinear modules, where each module elevates a level of information representation into a higher, more abstract level of representation, enables computer models to learn multiple-level representations of data [Paoletti, *et al.* (2018)]. A crucial problem that requires immediate resolution is how to combine deep learning technology with hyperspectral photography to provide intelligent information capture, processing, analysis, and comprehension. Researchers have employed deep learning algorithms extensively in the HSI categorization, particularly in the field of remote sensing [Li, *et al.* (2020)]. In the subject of medical HSI analysis, intelligently aided diagnosis enabled by deep learning offers a wide range of potential applications [Manni, *et al.* (2020)].

Feature extraction is used to extract the hidden features from the image. Convolutional Neural Networks (CNN), and Principal Component Analysis (PCA), is widely used feature extraction methods. CNN can be used for classification and also for feature extraction. CNN is having a convolutional layer, pooling layer, fully connected layer, softmax layer, and hidden layer [Guo, *et al.* (2022)]. To select the discriminative features from the extracted features, feature selection is used. Based on the availability of the label samples of the dataset, feature selection can be divided into the supervised method, semi-supervised method, and unsupervised method [Cao, *et al.* (2017)]. Supervised feature selection will use the maximum selective feature subgroups by calculating the significance of the class label. Clustering based feature selection method will extract the features by clustering the values. A novel graph-based clustering feature selection algorithm is proposed to improve the classification performance [Hufnagl & Lohninger (2020)].

Brain tumour classification is used to classify whether the tumour is a cancer tumour or a normal tumour. Supervised classification, unsupervised classification, and semi-supervised classification techniques are used to classify hyperspectral brain tumours. In supervised classification, the input and output values will be labelled values [Dong, *et al.* (2021)]. In unsupervised classification the unlabelled data is input, but the training model itself will create the labels and it will give the output [Lunga & Ersoy (2011)]. In semi-supervised classification, the input values are labelled and unlabelled samples [Chi & Bruzzone (2007)]. Semi-supervised classification methods are giving more classification accuracy for hyperspectral images. Because we can train the model by giving the labelled and unlabelled values. For hyperspectral images, a suggested graph-based semi-supervised learning classification approach is proposed.

The purpose of this research is to classify In-Vivo brain tumours using hyperspectral images and machine learning techniques, to achieve nearly 100% classification accuracy.

The balance of the paper is arranged as: The literature review is elaborated in section II, the proposed technique is introduced in section III, the dataset is described in section IV, and the experimental results are described in section V, along with a conclusion and recommendations for future research.

2. Literature Survey

To help neurosurgeons, to identify the boundaries of the tumour during resection, preventing the unnecessary removal of healthy tissue or the unintentional recurrence of the tumour. To achieve an effective result, a hybrid framework mixing supervised and unsupervised machine learning techniques are applied. First, a supervised pixel-by-pixel classification is performed using a Support Vector Machine classifier. The resulting classification

map is spatially homogenised by employing a one-band representation of the HS cube, the Fixed Reference t-Stochastic Neighbors Embedding dimensional reduction method, and the K-Nearest Neighbors filtering procedure [Fabelo, *et al.* (2018)].

The time cost and unpredictable outcomes of current dimensionality reduction strategies based on manifold embedding hinder final tissue categorization. A novel dimensionality reduction strategy and a new processing pipeline are created to provide a detailed tumour classification map for intraoperative margin determination during brain surgery. The suggested framework tries to address these issues through a two-step process: Dimensionality reduction is initially achieved using an adaptation of the T-distributed stochastic neighbour approach, followed by a semantic segmentation strategy for tissue categorization using a Semantic Texton Forest [Ravi, *et al.* (2017)].

The most prevalent primary brain malignant tumour is the glioblastoma (GBM) tumour. The accurate diagnosis of GBM tumours is crucial for both diagnosis and therapy. A modern medical detection technique called hyperspectral imaging is quick, non-contact, precise, and safe. It is anticipated to become a new intraoperative diagnosis tool. To fully utilise the spectral and spatial information of hyperspectral images (HSIs), a method based on the merging of many deep models is recommended for in vivo human brain HSI classification to obtain precise GBM tumour identification. To test the effectiveness of the suggested method, experiments are conducted on two real human brain hyperspectral datasets, each of which contains 36 in vivo HSIs collected from 16 different individuals. The proposed method has a 96.34% overall accuracy in identifying GBM tumours and a 96.69% accuracy in four-class classification [Hao, *et al.* (2021)].

Surgery for brain cancer's primary goal is to precisely remove the tumour while preserving as much of the patient's healthy brain tissue as is practical. A current clinical need is the creation of a non-contact, label-free technique to offer trustworthy assistance for tumour removal in real time during neurosurgery procedures. In this study, the authors provide a system for analysing hyperspectral images of human brain tissue in-vivo using deep learning. The suggested framework can provide a thematic map that shows the location of the tumour and the parenchymal region of the brain, guiding the operating surgeon toward a successful and accurate tumour removal. In terms of multiclass classification, the deep learning pipeline outperforms traditional support vector machine (SVM)-based techniques, achieving an overall accuracy of 80% [Fabelo, *et al.* (2019)].

To create models to assist in diagnosis, machine learning (ML) techniques are being integrated with HSI. Particularly during brain tumour surgery, the combination of these methods has been demonstrated to be trustworthy assistance in separating healthy tissue from malignant tissue. Machine learning (ML) methods such as random forests (RF), and support vector machines (SVM) and Deep learning (DL) methods such as convolutional neural networks (CNN) are used to produce predictions and offer in vivo visualisations that may improve the accuracy of neurosurgeons and assist protect healthy tissue. SVM, RF, and CNN classifiers were trained on thirteen in-vivo hyperspectral pictures from twelve separate patients with high-grade gliomas (grades III and IV). The examinations revealed five distinct categories: healthy tissue, tumour, venous blood vessel, arterial blood vessel, and dura mater [Urbanos, et al. (2021)].

The primary motive of this paper is to classify In-Vivo Brain cancer classification. This paper provides detailed information about the In-Vivo brain cancer images, and pre-processing techniques are used for pre-processing the In-Vivo brain cancer images after a multi-scale CNN features extraction method is used to extract the features from the pre-processed images. And graph-based clustering method is used to select the features from the extracted features. And semi-supervised graph-based classification method is used to get the classified output. And to combine the multi-scale CNN and semi-supervised graph convolutional network classification results in gradient boosting ensemble method is used.

3. Proposed Method

Applying deep learning techniques on human brain HSIs to detect GBM malignancies in vivo has received comparatively little research. There are still many challenges in this field. For instance, it is either expensive or time-consuming to get labelled samples of GBM tumours. As a result, there are often few training samples accessible in the medical industry. Then, segmentation algorithms are currently receiving greater attention in the area of brain tumour identification. The feature extraction of brain tumours may be more significant in practical applications because of the variations in the appearance of different levels and types of brain tumours. An important topic of research right now is the development of reliable and accurate feature extraction and classification algorithms for tumour identification. Furthermore, different deep networks are capable of extracting a variety of properties, including spectral, spatial, and spectral-spatial information. Additionally, various deep networks may extract a variety of properties, including spectral, spatial, and spectral-spatial features.

To overcome these challenges, we proposed a gradient boosting ensembled method (MCGC) for In-Vivo brain hyperspectral images. The following steps make up the majority of the proposed method: first, in-vivo brain picture pre-processing. Second, feature extraction using multi-scale CNN. Third, feature selection using a graph-based clustering method. Fourth, semi-supervised graph convolutional classification method. And finally, the output from the multiscale-CNN and output from the graph-based convolutional classification method is ensembled by using the gradient boosting ensembled method to get high classification accuracy. Figure 1 is

representing the detailed proposed architecture for gradient boosting ensembled method for In-Vivo brain tumour classification using hyperspectral images.

3.1. *Pre-processing*

It is a process of removing unwanted information from the image. In the hyperspectral medical imaging process also, we have the following pre-processing techniques: Data Normalization, Image Calibration, Noise Filtering, and Band Reduction.

3.1.1. Image calibration

The calibration phase is required to preserve the repeatability of the data despite the various surgical lighting conditions. To calibrate the images, the white and dark reference images must be taken. The white reference, which consistently reflects 95% of the incident light across the whole spectral range shielded by the employed hyperspectral cameras, is obtained using the Lambertian diffuse reflectance target. Covering the camera lens allows for the creation of the black reference. By covering the camera lens, the dark reference is obtained. In terms of white references, a capture is complete when the ceramic is positioned at the same distance from the in-vivo brain surface as the camera is pointed at and under the same lighting circumstances. Applying equation (1), to get a calibrated image. A calibrated image per band, C_I.

$$C_I = \frac{B_i C - B_i D}{B_i W - B_i D} \quad (1)$$

Here, the single band is represented by C, the dark reference is represented by D, and the white reference is represented by W.

3.1.2. Noise Filtering

It is used to remove the noise from the images.

3.1.3. Spectral Correction (band reduction)

Due to the great sensitivity of the snapshot camera, the response curves of the sensor show crosstalk at the peak wavelength of neighbours. This causes secondary harmonics in different curves that long- or short-pass filters cannot filter out. This effect can be reduced via the spectrum-correcting process. The signal must be multiplied by a correction matrix in order to produce the spectral-corrected image. By using equation (2), from the lower band to the higher bands are removed, they are from 0 to 50 bands and from 750 to 826 bands are removed using the band reduction.

$$R_b = C_I \times SCM \quad (2)$$

Here, C_I is the calibrated single band, and SCM is the correlation matrix.

3.1.4. Data Normalization

The normal brain's curved shape suggests that the picture pixels are not positioned at the same height, which causes a difference in the amount of light that the camera can collect. In this manner, the tissues will be identified in the photos based solely on the brightness of each pixel, disregarding the similarity of the spectral signatures. Utilizing data standardisation procedures that try to maintain the spectral signature form independent of the amplitude is important to lessen this impact. And also, it is used to prevent the non-uniform surface of the brain from producing varied radiation levels for each pixel. To normalise the coefficients in equation (3) and the spectral-corrected image cube in equation (4), the root mean square (RMS) values from spectral signatures across all bands are employed.

$$c[i,j] = \sqrt{\frac{\sum_{k=1}^{B}(R_b[i,j,k])^2}{B}} \quad (3)$$

$$I_{norm}[i,j,k] = \frac{R_b[i,j,k]}{c[i,j]} \quad (4)$$

Here, R_b is the cube with R, C, and B dimensions that have been spectrally corrected.

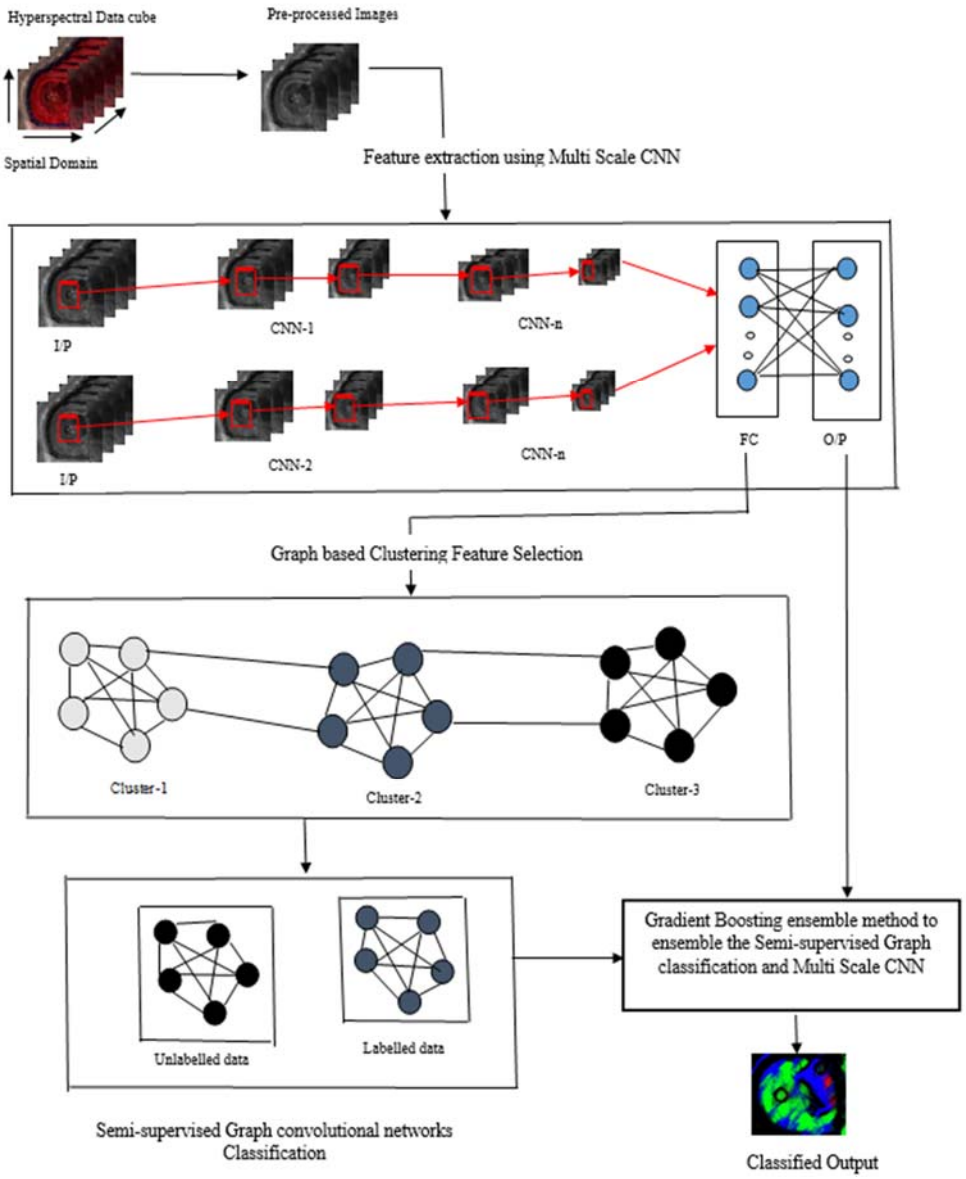

Fig. 1. Proposed (MCGC) Architecture of In-Vivo Brain Cancer Classification.

3.2. *Multi-Scale CNN based Feature Extraction*

Deep convolutional neural networks have garnered a lot of attention. Recently, due to their extraordinary capacity to extract the combined spectral-spatial information that results in accurately categorised images. Our proposed CNN design uses d×d×n input patches, where d is the spatial patches size and n is the count of bands in input. Given that the CNN network's performance is significantly influenced by the size of the spatial patches, d, the user should first identify the size of the spatial patches using a time-consuming, trial-and-error method. On the other hand, selecting the single optimal value for d might not be the best choice for depicting the scene in HSI that is supported by objects of various sizes. Furthermore, according to our research, not all types of information (spatial and spectral features) have the same optimal value for d. The magnitude of d is dependent on the kind of input data. To overcome these problems, different conventional multiscale frameworks are offered for the effective categorization of hyperspectral images.

Recently, various multiscale deep learning models have attracted interest in the categorization of remote sensing, which often has complicated structures and requires a lot of training data. We suggest, the multiscale CNN (MSCNN) in this work to overcome these problems. In figure 2, the architecture of multi-scale CNN is given. Our suggested deep model, known as MSCNN is equipped with a multiscale framework, with the requirement to seek the optimal value of d as well as the negative effects of utilising a single size value for d. Additionally, its features are the straightforward structure that produces sufficient accuracy results even in the presence of a depth of training examples. To counteract the impact of input patch size, MSCNN uses input patches that have varied sizes

around each pixel. The classification probability maps generated by the SoftMax function for each input are combined with the feature extraction results using the gradient boosting ensembled method.

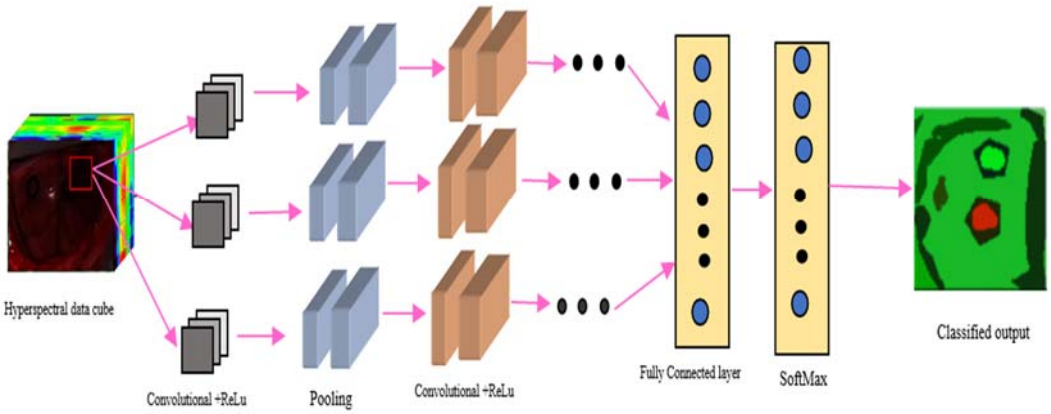

Fig. 2. Architecture of multiscale-CNN.

To extract the features from an image we have proposed a Multi-scale CNN method. And the final classified output of the multi-scale CNN is used for the classification. We pass the input image to the convolutional layer, which will conduct the mathematical process represented by the multiplication of an image matrix and a filter kernel. The activation layer will be the Rectified Linear Unit (ReLU), which will transform negative values into non-negative ones. By reducing the convolution layer's output pixels, the pooling layer is used to reduce the complexity of large photographs. The feed-forward networks are built on a fully linked layer. The fully connected layer receives its input from the pooling layer's output. And then a fully connected layer will provide the image's extracted features. Softmax layer will accept any input values such as negative, positive, zero, or larger than one, however soft max layer will not accept negative, positive, zero, or greater than one. And the output of the softmax layer will be the classified output of the brain cancer classification.

Convolutional layer feature maps

$$h_{i,j} = \sum_{k=1}^{m} \sum_{l=1}^{m} w_{k,l} x_{i+k-1,j+l-1} \quad (5)$$

Max Pooling layer:

$$h_{i,j} = \max\{x_{i+k-1,j+l-1,\forall \le k \le m \text{ and } 1 \le l \le m}\} \quad (6)$$

3.3. *Graph-based Clustering for Feature (band) Selection*

Feature (band) selection is described as a graph-based problem in graph theory, where nodes in a graph represent the HSI bands and edges between nodes indicate how similar two bands are to one another. To identify representative bands, a graph-based clustering approach creates an affinity matrix A, that corresponds with band similarity. Each affinity between the pairwise band is calculated as $a_{i,j} = \exp(-f_i - f_j / 2\sigma^2)$, with σ signifying a scaling factor. Specifically, A is a matrix that specifies band affinities. Spectral clustering is a common example of a graph-based clustering technique. That makes clustering on the stacking eigenvectors of the affinity matrix Γ, defined in equation (7),

$$L = \Lambda^{-1/2} \Gamma \Lambda^{-1/2} \quad (7)$$

Here, L represents the normalized graph Laplacian, and ∧ represents the diagonal matrix computed by the sums over the rows of A.

The bands are chosen from the retrieved features using the feature (band) selection procedure. Clustering is a process of splitting a set of data points in the same group that are more similar than data points in another group. Graph-based clustering method will create the graph G = (V, E, W) by using the extracted features. Here, V is vertices, E is edges, and W is weight. And then it will start the feature (band) selection by applying the k-means clustering, and then it will choose the centroid of each cluster as a representative, K = $\{x_1, x_2, \ldots \ldots \ldots \ldots, x_n\}$ and the distance between the edges will be calculated by using Euclidean distance. And then similar features (F_s) will be selected.

$$\text{Euclidean distance} = D(x, y) = \sqrt{\sum_{i=1}^{n} (y_j - x_i)^2} \quad (8)$$

Algorithm: Gradient boosting ensembled classification method for In-Vivo Brain cancer classification

1. Image cube generation
2. Brain Cancer Images $\boldsymbol{B_i}$
3. Image calibration

$$\boldsymbol{C_I = \frac{B_i C - B_i D}{B_i W - B_i D}}$$

4. Spectral Correction
$$\boldsymbol{I_{sc} = C_I * SCM}$$
5. Normalization
$$\boldsymbol{c[i,j]} = \sqrt{\frac{\sum_{k=1}^{B}(Isc[i,j,k])^2}{B}}$$
$$\boldsymbol{I_{norm}[i,j,k]} = \frac{\boldsymbol{I_{sc}[i,j,k]}}{\boldsymbol{c[i,j]}}$$
6. Pre-processed output $\boldsymbol{p_i}$
7. $\boldsymbol{p_i}$ to the convolutional layer size (h× $\boldsymbol{w \times k}$)
8. Convolutional layer feature maps
$$\boldsymbol{h_{i,j} = \sum_{k=1}^{m}\sum_{l=1}^{m} w_{k,l} x_{i+k-1,j+l-1}}$$
9. Max Pooling layer:
$$\boldsymbol{h_{i,j} = \max\{x_{i+k-1,j+l-1,\forall \le k \le m \text{ and } 1 \le l \le m}\}}$$
10. Fully connected layer: extracted features $\boldsymbol{F_e}$
11. SoftMax layer: classified output $\boldsymbol{C_o}$
12. Constructing a graph by using the extracted features $\boldsymbol{F_e}$
13. Graph G= (V, E, W)
14. Input V = $\{\boldsymbol{v_1, v_2, \dots\dots\dots, v_n}\}$
15. Starting a feature (band) selection by using the k-means clustering, and choosing the centroid of each cluster as representative.
K = $\{\boldsymbol{x_1, x_2, \dots\dots\dots\dots, x_n}\}$
16. By checking the distance between the connected points d $(\boldsymbol{x_i, x_j})$ is computed as the Euclidean distance between the nodes
D (x, y) = $\sqrt{\sum_{i=1}^{n}(\boldsymbol{y_j - x_i})^2}$
17. Selecting similar features (bands) from the graph $\boldsymbol{F_s}$
18. By using the selected features (bands) $\boldsymbol{F_s}$, constructing a semi-supervised graph convolutional network
Labelled data $\boldsymbol{F_l = \{f_1, f, \dots\dots\dots, f_n\}}$
Unlabelled data $\boldsymbol{S_u = \{s_1, s_2, \dots\dots\dots, s_n\}}$
19. Creating the class labels $\boldsymbol{C = [C_1, C_2, \dots\dots\dots, C_n]}$
C is denoted by $\boldsymbol{y_l \in R^{c \times l}}$ with $\boldsymbol{y_{ij} = 1 \; if \; x_j \in c_j}$
20. Divide the training data points $\boldsymbol{Z = [X_l, S_u]}$ will produce the weighted graph G = (V, E)
where, V consists of N = l + u data points $\boldsymbol{E \in R^{N \times N}}$ is the adjacency matrix
21. Laplacian matrix is obtained by L = D-A
Where D is the diagonal matrix given by $\boldsymbol{D_{ii} = \sum_j w_{ij}}$
22. C to the convolutional layer size (d × b × s)
23. Convolutional layer feature maps
$$\boldsymbol{d_{i,j} = \sum_{k=1}^{m}\sum_{l=1}^{m} b_{k,l} n_{i+k-1,j+l-1}}$$
24. Max pooling layer:
$$\boldsymbol{d_{i,j} = \max\{n_{i+k-1,j+l-1,\forall \le k \le m \text{ and } 1 \le l \le m}\}}$$
25. Fully connected layer
26. SoftMax layer: Classified graph $\boldsymbol{T_g}$
27. Classified output $\boldsymbol{C_o}$, Classified graph $\boldsymbol{T_g}$
28. Minimize the loss function
$$\boldsymbol{L = fun(F(X_1), F(X_2), \dots\dots\dots, F(X_n))}$$
29. Minimization is performed by fitting an estimator H on $(\boldsymbol{X_n}, \frac{\partial \boldsymbol{L}}{\partial \boldsymbol{X_i}})\ \forall_i$
F(X)+H(X) is an approximation of gradient descent $\boldsymbol{F(X_i) = F(X_i) - \frac{\partial L}{\partial F(X_i)}}$
30. Brain tumour classification results.

3.4. *Semi-supervised Graph Convolutional Network Classification*

3.4.1. Basics to construct a graph

The definition of a semi-supervised graph convolutional network is G = (V, E), where V denotes the graph's vertices and E denotes its edges. An adjacency matrix is denoted by $A = [a_{i,j}] \in R^{N\times N}$. The degree of a matrix of A is $D = diag(d_1, d_2, \ldots\ldots d_N)$, where $d_i = \sum_j a_{ij}$. L = D – A is defined for laplacian. and $\mathcal{L} \coloneqq I_N - D^{\frac{-1}{2}} A D^{\frac{-1}{2}}$, is the formula for normalised graph Laplacian. Here I_N is the identity matrix.
Spectral Graph signal $x \in R^N$ (one scalar for each node) and spectral filter g_θ, which is a function of L's eigenvalues, are multiplied by CNNs to create convolution. Inconvenient for big graphs, this approach is essential for locating the Laplacian matrix's eigenvectors. One solution to this problem is to approximate the spectral filter g_θ, with Chebyshev polynomials up to the K_{th} order is one technique to get around this issue. Creating the K-localized ChebNet with the following definition of convolution:

$$g_\theta{}' * x \approx \sum_{k=0}^{k} \theta'_k T_k(\mathcal{L}) x \quad (9)$$

Here, $x \in R^N$ represents the signal of the graph, $g_\theta{}'$ represents the spectral filter, * represents the convolutional operator, T_k represents Chebyshev polynomials, $\mathcal{L} = \frac{2}{\lambda_{max}}\mathcal{L} - I_N$, were λ_{max} denotes the largest eigenvalue of $\mathcal{L}$, $\theta' \in R^k$ is a vector of coefficients for Chebyshev. Here, k=1 is to simplify an approximation and model λ_{max} of $\mathcal{L}$ by 2. And then, the convolution becomes

$$g_\theta * x = \theta\,(I_N + D^{\frac{-1}{2}} A D^{\frac{-1}{2}}) x \quad (10)$$

Here, Θ is the Chebyshev coefficient. Also, included a normalising method and used the convolution matrix as the subject.

$$I_N + D^{\frac{-1}{2}} A D^{\frac{-1}{2}} \rightarrow D^{\frac{-1}{2}} \tilde{A} D^{\frac{-1}{2}} \quad (11)$$

Here, $\tilde{A} = A + I_N$ and $D_{ij} = \sum_j \tilde{A}_{ij}$. Applying the previously mentioned concept of convolution to the graph signal i.e., $X \in R^{N\times C}$ (A C-dimensional feature vector connects each node in this aided model), and its propagation model is:

$$H^{l+1} = \delta\,(D^{\frac{-1}{2}} \tilde{A} D^{\frac{-1}{2}} H^{(l)} W^{(l)}) \quad (12)$$

Here, $H^{(l)}$ is representing the matrix of activation functions in the layer l, and $H^0 = X, W^{(l)}$ represents the activation function is referenced by the trainable weight matrix in layer l, δ refers to the activation function (e.g., ReLU (.) = max (0,.)). This model is called the graph convolutional network (GCNs). And then we have to apply the SoftMax function to get the classification output

$$Z = softmax\,(\tilde{A} ReLU(\tilde{A} X W^0) W^{(l)}) \quad (13)$$

Here, $\tilde{A} = D^{\frac{-1}{2}} \tilde{A} D^{\frac{-1}{2}}$, SoftMax $(x_i) = \frac{\exp(x_i)}{\sum_i \exp(x_i)}$. The cross-entropy error over all labelled samples is the loss function.

$$L \coloneqq -\sum_{l\in y_L} \sum_{f=1}^{F} Y_{lf} ln Z_{lf} \quad (14)$$

Here, y_L represents the collection of node indices with labels, and F, which is equal to the number of classes, denotes the number of nodes in the output layer. And $Y \in R^{|y_L|\times F}$ represents the label indicator matrix. The GCN model convolutionally associates graph structures and node characteristics unlabelled node features are combined with those of surrounding labelled nodes, and the graph is propagated via many layers. The graph convolutional network architecture is shown in figure 3.

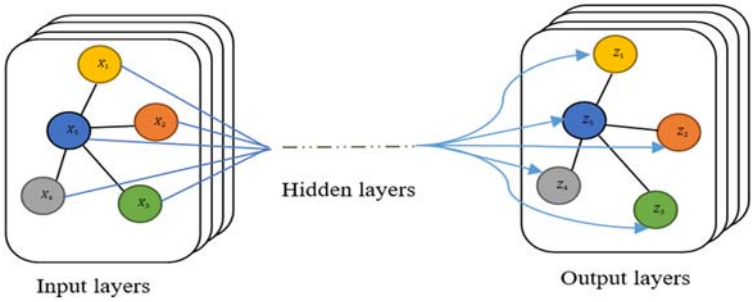

Fig. 3. Graph convolutional network architecture.

Brain cancer is categorised using a semi-supervised graph convolutional network (GCN) based classification approach. Semi-supervised graph convolutional network will take both labelled and unlabelled samples as the input. Labelled samples are represented as $F_l = \{f_1, f_2, \ldots\ldots\ldots, f_n\}$, unlabelled samples are represented as $S_u =$

$\{s_1, s_2, \ldots\ldots\ldots, s_n\}$. By using these labelled samples and unlabelled samples, we are creating a class C, $C = [C_1, C_2, \ldots\ldots\ldots, C_n]$. C is denoted by $y_l \in R^{c\times l}$ with $y_{ij} = 1\ if\ x_j \in c_j$. And then, we have to define the class values in training and testing. The training data points $Z = [X_l, S_u]$ will generate the weighted graph G = (V, E). and then the number of spanning trees is counted by using the Laplacian matrix. Laplacian matrix L = D – A. here, the diagonal matrix is D, and it is given by $D_{ii} = \sum_j w_{ij}$. And that generated graph will send the input, and ReLU is used as an activation function to remove the non-zero values. And SoftMax function will give the classified output.

3.5. *Gradient Boosting Ensembled Classification*

A homogeneous ensemble learning algorithm transforms numerous weak learners into strong learners. To create a stronger and more complete strong monitoring model, ensemble learning is used to merge many weak monitoring models. One of the ensemble algorithms is the boosting method. Learning numerous classifiers and linearly combining these classifiers, by changing the weight of the training data, improves classifier performance (raising the weight of the error-corrected samples and decreasing the weight of the paired samples). One kind of boosting technique is gradient boosting. Its main tenet is to generate a new model each time using the gradient of the prior model's loss function.

The gradient boosting ensemble method will be used to ensemble the classification models. It will take the difference between the prediction value and the ground truth of the classified models. Here, we are taking the multi-scale CNN model classified out and semi-supervised graph-based classification output to the ensemble by using the gradient boosting ensemble method. First, it will minimize the loss function and then the minimization is performed by an estimator, and then the approximation of gradient descent will be calculated. Gradient descent (GD) is an iterative first-order optimisation process for locating a function's local minimum/maximum. After that, we can get whether the patient is having a brain cancer tumour or a non-cancer tumour as the output.

Minimize the loss function:

$$L = fun(F(X_1), F(X_2), \ldots\ldots\ldots, F(X_n)) \quad (15)$$

Minimization is performed by fitting an estimator H on $(X_n, \frac{\partial L}{\partial X_i})\ \forall_i$

F(X)+H(X) is an approximation of gradient descent $F(X_i) = F(X_i) - \frac{\partial L}{\partial F(X_i)}$ (16)

4. Dataset Description

These images are of adult patients who had craniotomies to remove intra-axial brain lesions. Images were collected on five different patients with grade IV glioblastoma tumours that were verified on histology at the University Hospital Doctor Negrin in Las Palmas de Gran Canaria, Spain, and the University Hospital of Southampton, United Kingdom. To collect in-vivo data, the neurosurgeons must first put some rubber ring markers on the brain's surface. When the macroscopic look of the tissue inside the markers gives them confidence that it is cancer or normal tissue. Moreover, information from an MRI scan was obtained following the craniotomy and durotomy and relayed by the neuro navigator (Magnetic Resonance Image). Visual and near-infrared sensors are used to take pictures of in-vivo brain cancer (VNIR). The range of wavelengths is 400 to 1000 nm [Fabelo, *et al.* (2019)]. 36 hyperspectral pictures altogether from 22 distinct patients were gathered. Using this data, 30000 and more spectral signatures were labelled using the spectral angular mapper (SAM). Additionally, four categories were established, including background elements, blood vessels, normal tissue, and tumour tissue. Table 1 will show the details of the database.

Table 1. Details of In-Vivo brain cancer database.

Image ID	No. of Pixels	Dimensions (H×W×B)	Size [MB]
P1C2	264,408	479×552×826	428.23
P3C1	184,875	375×493×826	299.65
P1C1	251,532	459×548×826	407.41
P2C1	219,232	442×496×826	355.19
P4C1	124,033	377×329×826	201.24

5. Evaluation Metrics

After classifying either validation or test data after training models for each approach, a confusion matrix is immediately generated. To choose the best models, the overall accuracy (OACC) measure is computed using the confusion matrix. Ultimately employ the chosen one to categorise fresh photos, this is done during the cross-validation [Urbanos, *et al.* (2021)]. To get the classification accuracy for hyperspectral In-Vivo Brain cancer image classification, we have the following evaluation metrics: Sensitivity, Specificity, and Overall Accuracy [SAE Rahman (2015)]. To evaluate a model and to predict the true positives from each available category

sensitivity evaluation metric is used. To evaluate a model and to predict the true negatives from each category specificity evaluation metric will be used. Accuracy is used to calculate how the model is performing across the classes. According to [Fabelo, *et al.* (2018)], The following criteria are used to evaluate performance: true positive, false positive, true negative, and false positive.

- True Positive (TP): the perfect circumstances were recognised. The test produced a positive result, and the real value of the categorization is similarly positive.
- False Positive (FP): True negatives are conditions that were incorrectly detected. Test findings are unfavourable, and the classification value is favourable.
- True Negative (TN): Conditions have been successfully refused. The test results are unfavourable, and this is reflected in the classification value.
- False Negative (FN): False negative conditions are those that were improperly rejected. The test results are favourable, whereas the classification values are unfavourable.

$$Sensitivity: \frac{TP}{TP+FN} \tag{10}$$

$$Specificity: \frac{TN}{TN+FP} \tag{11}$$

$$Accuracy: \frac{TP+TN}{TP+FP+TN+FN} \tag{12}$$

6. Experimental Results

To determine the efficiency of the MGCN method, the studies employ a leave-one-patient-out cross-validation method. Testing is done using the labelled samples seen in images of a patient with GBM tumour tissue, and training is done using the unlabelled samples from additional patients. These seven HSIs from five patients with Grade IV GBM tumours are utilised to gauge how well the suggested approach performs at categorization. To validate the presence of the proposed MGCN model we have contrasted the random forest and support vector machine methods [LuisaRuiz, *et al.* (2020)]. And we performed the classification by using the In-Vivo brain cancer image database. The dataset description is given in Table 1. categorization precision of the suggested approach is shown in figure 4, and the classified accuracy with a comparison of existing models is shown in table 2. Figure 5, is showing that the classification accuracy of the proposed method. Specificity and sensitivity are shown in figure 6, figure 7. Our proposed method achieved 100% accuracy of the existing methods.

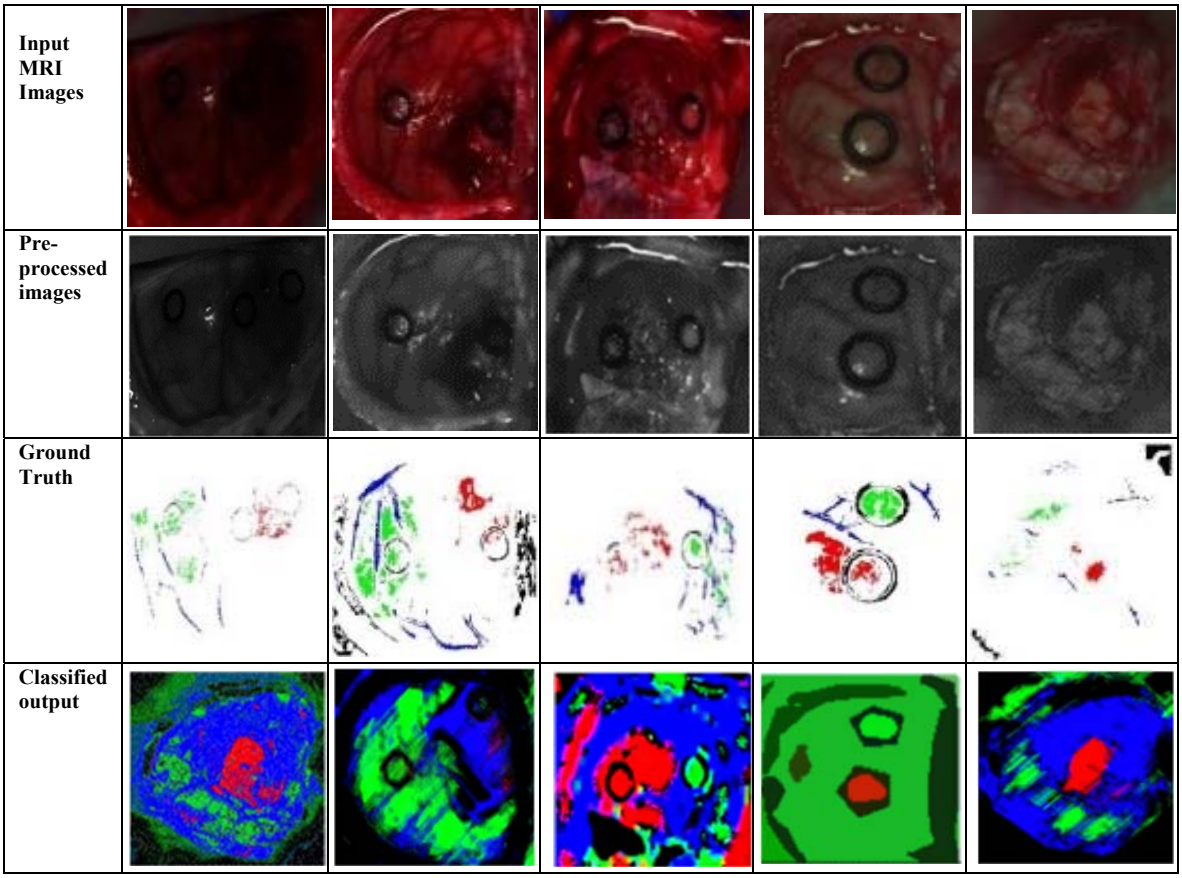

Fig. 4. Classified results of In-Vivo Brain cancer database.

The brain tumour part is represented with red colour and the non-tumour region is represented with green colour.

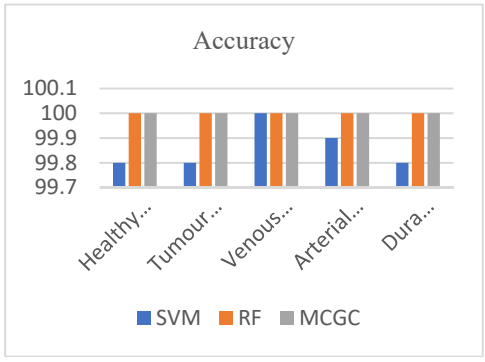

Fig. 5. Classified accuracy.

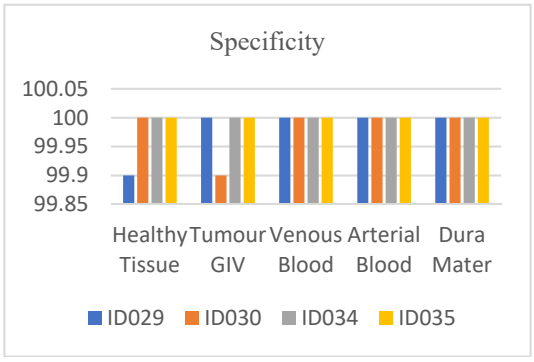

Fig. 6. Specificity.

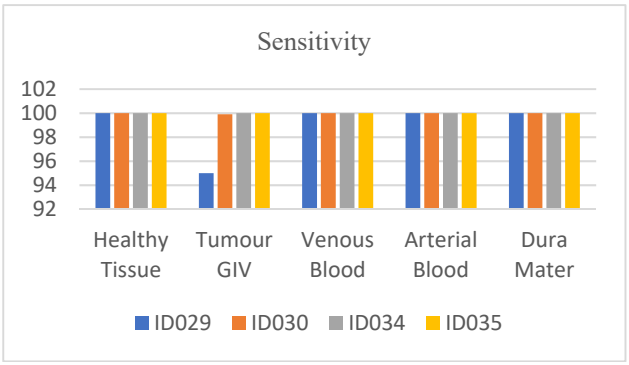

Fig. 7. Sensitivity.

Table 2. Accuracy of SVM, RF, and proposed MCGC

	P1C2	P3C1	P1C1	P4C1
SVM	99.8	99.8	100	99.8
RF	100	100	100	100
MCGN	99.9	100	100	100

7. Conclusions and Future work

Medical image classification using hyperspectral images is one of the difficult tasks due to the limited datasets. By using hyperspectral images, we can classify the disease in its early stage. By using hyperspectral medical image classification, we can classify skin cancer, tissue classification, and cell classification. In this article, we have proposed a gradient-boosting ensembled classification (MCGC) method to classify In-Vivo Brain cancer. The proposed algorithms have achieved satisfactory results. Because here we have performed the multi-scale CNN and Graph-based clustering method for feature extraction and feature (band) selection. And we have used the In-Vivo Brain cancer database to classify the brain tumour. These database images are created by using the VNIR sensor and the wavelength is from 400 to 700nm. The evaluation metrics are calculated by using accuracy, specificity and sensitivity, the proposed method achieves good results. And in future, we have to extend this work with more In-Vivo brain tumour hyperspectral images.

Conflict of Interest

The authors have no conflicts of interest to declare. The article interpretation and analysis were contributed to by all authors, who also drafted the substantial scientific content.

References

[1] Andria, G., Attivissimo, F., Cavone, G., & Lanzolla, A. M. (2009). Acquisition times in magnetic resonance imaging: optimization in clinical use. *IEEE Transactions on Instrumentation and Measurement 58*, 3140-3148.
[2] Arnold, T., Biasio, M. D., & Leitner, R. (2010). High-sensitivity hyper-spectral video endoscopy system for intra-surgical tissue classification. *In SENSORS*.
[3] Bajwa, S. G., Bajcsy, P., Groves, P., & Tian, L. F. (2004). Hyperspectral image data mining for band selection in agricultural applications. *Transactions of the ASAE 47*.
[4] C.Tiwari, K., Arora, M. K., & Singh, D. (2011). An assessment of independent component analysis for detection of military targets from hyperspectral images. *nternational Journal of Applied Earth Observation and Geoinformation 13*.
[5] Calin, M. A., Parasca, S. V., Savastru, D., & Manea, D. (2014). Hyperspectral imaging in the medical field: Present and future. *Applied Spectroscopy Reviews 49*.
[6] Calin, M. A., Parasca, S. V., Savastru, D., & Manea., D. (2014). Hyperspectral imaging in the medical field: Present and future. *Applied Spectroscopy Reviews 49*, 435-447.
[7] Cao, X., Wei, C., Han, J., & Jiao, L. (2017). Hyperspectral band selection using improved classification map. *IEEE geoscience and remote sensing letters 14*.
[8] Chi, M., & Bruzzone, L. (2007). Semisupervised classification of hyperspectral images by SVMs optimized in the primal. *IEEE Transactions on Geoscience and Remote Sensing 45*.
[9] Dong, S., Quan, Y., Feng, W., Dauphin, G., Gao, L., & Xing, M. (2021). A Pixel Cluster CNN and Spectral-Spatial Fusion Algorithm for Hyperspectral Image Classification With Small-Size Training Samples. *IEEE Journal of Selected Topics in Applied Earth Observations and Remote Sensing 14* .
[10] Fabelo, H., Halicek, M., Ortega, S., Shahedi, M., Szolna, A., Piñeiro, J. F., & al, C. S. (2019). Deep learning-based framework for in vivo identification of glioblastoma tumor using hyperspectral images of human brain. *Sensors 19*, 920.
[11] Fabelo, H., Ortega, S., Lazcano, R., Madroñal, D., Callicó, G. M., Juárez, E., & al, R. S. (2018). An intraoperative visualization system using hyperspectral imaging to aid in brain tumor delineation. *Sensors 18*, 430.
[12] Fabelo, H., Ortega, S., Ravi, D., Kiran, B. R., Sosa, C., Bulters, D., & a, G. M. (2018). Spatio-spectral classification of hyperspectral images for brain cancer detection during surgical operations. *PloS one*.
[13] Fabelo, H., Ortega, S., Szolna, A., Bulters, D., Piñeiro, J. F., Kabwama, S., & al, A. J. (2019). In-vivo hyperspectral human brain image database for brain cancer detection. *IEEE Access 7*, 39098-39116.
[14] Florimbi, G., Fabelo, H., Torti, E., Ortega, S., Marrero-Martin, M., Callico, G. M., . . . Leporati, F. (2020). Towards real-time computing of intraoperative hyperspectral imaging for brain cancer detection using multi-GPU platforms. *EEE Access 8*, 8485-8501.
[15] Guo, W., Xu, G., Liu, B., & Wang, Y. (2022). Hyperspectral Image Classification Using CNN-Enhanced Multi-Level Haar Wavelet Features Fusion Network. *IEEE Geoscience and Remote Sensing Letters 19*, 1-5.
[16] Hao, Q., Li, S., & Kang, X. (2020). Multilabel sample augmentation-based hyperspectral image classification. *IEEE Transactions on Geoscience and Remote Sensing 58*, 4263-4278.
[17] Hao, Q., Pei, Y., Zhou, R., Sun, B., Sun, J., Li, S., & Kang, X. (2021). Fusing multiple deep models for in vivo human brain hyperspectral image classification to identify glioblastoma tumor. *IEEE Transactions on Instrumentation and Measurement 70*, 1-14.
[18] Huang, N., Xiao, L., Xu, Y., & Chanussot., J. (2021). A Bipartite Graph Partition-Based Coclustering Approach With Graph Nonnegative Matrix Factorization for Large Hyperspectral Images. *EEE Transactions on Geoscience and Remote Sensing*.
[19] Hufnagl, B., & Lohninger, H. (2020). A graph-based clustering method with special focus on hyperspectral imaging. *Analytica chimica acta 1097*.
[20] Jamshidpour, N., Homayouni, S., & Safari, A. (2016). Graph-based semi-supervised hyperspectral image classification using spatial information. *th Workshop on Hyperspectral Image and Signal Processing: Evolution in Remote Sensing (WHISPERS)*.
[21] Kanthi, M., Sarma, T. H., & Bindu, C. S. (2020). A 3D-deep CNN based feature extraction and hyperspectral image classification. *IEEE India Geoscience and Remote Sensing Symposium (InGARSS)*, 229-232.
[22] Khan, M. J., Khan, H. S., Yousaf, A., Khurshid, K., & Abba, A. (2018). Modern trends in hyperspectral image analysis: A review. *Ieee Access 6*, 14118-14129.
[23] Lazcano, R., Madroñal, D., Florimbi, G., Sancho, J., Sanchez, S., Leon, R., & al, H. F. (2019). Parallel Implementations Assessment of a Spatial-Spectral Classifier for Hyperspectral Clinical Applications. *IEEE Access 7*, 152316-152333.
[24] LeCun, Y., Bengio, Y., & Hinton, G. (2015). Deep learning. *nature 521*, 436-444.
[25] Lee, H., & Kwon, H. (2017). Going deeper with contextual CNN for hyperspectral image classification. *IEEE Transactions on Image Processing 26*.
[26] Lefei Zhang, Zhang, Q., Du, B., Huang, X., Tang, Y. Y., & Tao, D. (2016). Simultaneous spectral-spatial feature selection and extraction for hyperspectral images. *IEEE Transactions on Cybernetics 48*.
[27] Li, R., Zheng, S., Duan, C., Yang, Y., & Wang, X. (2020). Classification of hyperspectral image based on double-branch dual-attention mechanism network. *Remote Sensing 12*, 582.
[28] Lu, G., Halig, L., Wang, D., Chen, Z. G., & Fei, B. (2014). Hyperspectral imaging for cancer surgical margin delineation: registration of hyperspectral and histological images. *International Society for Optics and Photonics, 9036*.
[29] LuisaRuiz, Martín, A., Urbanos, G., Villanueva, M., Sancho, J., Rosa, G., & al, M. V. (2020). Multiclass Brain Tumor Classification Using Hyperspectral Imaging and Supervised Machine Learning. *Conference on Design of Circuits and Integrated Systems*.
[30] Lunga, D., & Ersoy, O. (2011). "Unsupervised classification of hyperspectral images on spherical manifolds. *In Industrial Conference on Data Mining*.
[31] Ma, L., Lu, G., Wang, D., Wang, X., Chen, Z. G., Muller, S., . . . Fei, B. (2017). Deep learning based classification for head and neck cancer detection with hyperspectral imaging in an animal model. *In Medical imaging 2017: Biomedical applications in molecular, structural, and functional imaging*.
[32] Ma, L., Ma, A., Ju, C., & Li, X. (2016). Graph-based semi-supervised learning for spectral-spatial hyperspectral image classification. *pattern recognition letters 83*.
[33] Manni, F., Sommen, F. v., Fabelo, H., Zinger, S., Shan, C., Edström, E., . . . With, P. H. (2020). Hyperspectral imaging for glioblastoma surgery: Improving tumor identification using a deep spectral-spatial approach. *Sensors 20*, 6955.
[34] Paoletti, M. E., Haut, J. M., Fernandez-Beltran, R., Plaza, J., Plaza, A. J., & Pla, F. (2018). Deep pyramidal residual networks for spectral–spatial hyperspectral image classification. *IEEE Transactions on Geoscience and Remote Sensing 57*, 740-754.
[35] Petropoulos, G. P., Kalivas, D. P., Georgopoulou, I. A., & Srivastava, P. K. (2015). Urban vegetation cover extraction from hyperspectral imagery and geographic information system spatial analysis techniques: case of Athens, Greece. *ournal of Applied Remote Sensing 9*.
[36] Pike, R., Lu, G., Wang, D., Chen, Z. G., & Fei, B. (2015). A minimum spanning forest-based method for noninvasive cancer detection with hyperspectral imaging. *IEEE Transactions on Biomedical Engineering 63*, 653-663.

[37] Rahman, S. A. (n.d.). Hyperspectral imaging classification using ISODATA algorithm;.
[38] Ravi, D., Fabelo, H., Callic, G. M., & Yang, G.-Z. (2017). Manifold embedding and semantic segmentation for intraoperative guidance with hyperspectral brain imaging. *IEEE transactions on medical imaging 36*, 1845-1857.
[39] Ravi, D., Fabelo, H., Callic, G. M., & Yang, G.-Z. (2017). Manifold embedding and semantic segmentation for intraoperative guidance with hyperspectral brain imaging. *IEEE transactions on medical imaging 36*, 1845-1857.
[40] Ross, B. J., Gualtieri, A. G., Fueten, F., & Budkewitsch, P. (2005). Hyperspectral image analysis using genetic programming. *Applied Soft Computing 5*.
[41] Sakla, W., Chan, A., Ji, J., & Sakla, A. (2010). An SVDD-based algorithm for target detection in hyperspectral imagery. *IEEE Geoscience and Remote Sensing Letters 8*.
[42] Sancho, J., Urbanos, G., Ruiz, L., Villanueva, M., Rosa, G., Diaz, A., & al, M. V. (2020). Towards GPU Accelerated HyperSpectral Depth Estimation in Medical Applications. *Conference on Design of Circuits and Integrated Systems (DCIS).*
[43] Souza, M. M., Carvalho, F. A., Sverzut, E. F., Requena, M. B., Garcia, M. R., & Pratavieira, S. (2021). Hyperspectral Imaging System for Tissue Classification in H&E-Stained Histological Slides. *SBFoton International Optics and Photonics Conference (SBFoton IOPC).*
[44] Urbanos, G., Martín, A., Vázquez, G., Villanueva, M., Villa, M., Jimenez-Roldan, L., . . . Sanz, C. (2021). Supervised machine learning methods and hyperspectral imaging techniques jointly applied for brain cancer classification. *Sensors 21*, 3827.
[45] Urbanos, G., Martín, A., Vázquez, G., Villanueva, M., Villa, M., Jimenez-Roldan, L., . . . Sanz, C. (2021). Supervised machine learning methods and hyperspectral imaging techniques jointly applied for brain cancer classification. *Sensors 21*, 3827.
[46] Wang, J., Sun, K., Cheng, T., Jiang, B., Deng, C., Zhao, Y., & al, D. L. (2020). Deep high-resolution representation learning for visual recognition. *IEEE transactions on pattern analysis and machine intelligence 43*, 3349-3364.
[47] Wei, X., Li, W., Zhang, M., & Li, Q. (2019). Medical hyperspectral image classification based on end-to-end fusion deep neural network. *EEE Transactions on Instrumentation and Measurement 68*.
[48] Wei, Y., Xia, W., Lin, M., Huang, J., Ni, B., Dong, J., . . . Yan, S. (2015). HCP: A flexible CNN framework for multi-label image classification. *IEEE transactions on pattern analysis and machine intelligence 38*, 1901-1907.
[49] Ye, M., Ji, C., Chen, H., Lei, L., Lu, H., & Qian, Y. (2020). Residual deep PCA-based feature extraction for hyperspectral image classification. *Neural Computing and Applications 32*.
[50] Zhang, X., Jiang, X., Jiang, J., Zhang, Y., Liu, X., & Cai, Z. (2021). Spectral–Spatial and Superpixelwise PCA for Unsupervised Feature Extraction of Hyperspectral Imagery. *IEEE Transactions on Geoscience and Remote Sensing 60*, 1-10.

Authors Profile

Ganji Tejasree, is pursuing her PhD at the School of Information Technology and Engineering, Vellore Institute of Technology Vellore. She completed her bachelor of engineering degree in Computer Science and Engineering from Chaitanya Bharathi Institute of Technology (Autonomous, affiliated to Osmania University), Hyderabad in the year 2018 and her Master of Technology from Vardhaman College of Engineering (Affiliated to Jawaharlal Nehru Technology University Hyderabad), Hyderabad in the year 2020. Her research interest is Hyperspectral Image Processing, Machine Learning, and Deep Learning.

L Agilandeeswari completed her PhD and working as Associate Professor in the School of Information Technology & Engineering (SITE), VIT Vellore. She received her Bachelor's degree in Information Technology and Master's in Computer Science and Engineering from Anna University in 2005 and 2009 respectively. She is having around 14+ years of teaching experience and published 50+ papers in peer-reviewed reputed journals. Her reputed publications include research articles in peer-reviewed journals namely Expert Systems with Applications, IEEE Access, Journal of Ambient Intelligence and Humanized Computing, Multimedia Tools and Applications, and Journal of Applied Remote Sensing indexing at Thomson Reuters with an average impact factor of 5. She is a peer reviewer in journals including IEEE Access, Pattern Recognition, International Journal of Remote Sensing, Array, Artificial Intelligence Review, Informatics in Medicine Unlocked, Neurocomputing, Computers, and Electrical Engineering, Journal of King Saud University– Computer and Information Sciences, IET ReView, Journal of Engineering Science and Technology (JESTEC), etc. She also published about 13 engineering books as per Anna University Syllabus. Her areas of interest include Image and video watermarking, Image processing, Neural networks, Cryptography Fuzzy Logic, Machine Learning, IoT, Information-Centric Networks, and Remote Sensing.